American Journal of Remote Sensing
2025, Vol. 13, No. 2, pp. 87-99
https://doi.org/10.11648/j.ajrs.20251302.13

Research Article

Study and Modeling of a Photon-counting DIAL (Differential Absorption Lidar) System Applied to the Detection of Tropospheric Gas Molecules

Hajanirina Jean Emile Randrianjatovo[1, *], Hariniony Bienvenu Rakotonirina[2], Marie Emile Randrianandrasana[2]

[1]Doctoral Schools in Sciences and Engineering Techniques and Innovation, University of Antananarivo, Antananarivo, Madagascar

[2]High School Polytechnics of Antsirabe, University of Vakinankaratra, Antsirabe, Madagascar

Abstract

The Differential Absorption Lidar (DIAL) technique is one of the most effective methods for detecting atmospheric gases. It is based on the interaction between laser-emitted light and atmospheric molecules. The backscattered optical signal is converted into an electrical signal using photomultiplier tubes or other types of detectors. Two main detection approaches are commonly used: analog detection and photon-counting detection. While the analog mode is widely employed, it suffers from limited sensitivity. The photon-counting mode, although more suitable for detecting extremely weak signals, faces challenges in daytime measurements due to strong solar background noise. The main objective of this study is to evaluate the performance of the photon-counting technique to enable the DIAL system to detect extremely weak optical signals. To this end, modeling and simulation of the parameters influencing system performance have been carried out. Furthermore, the impact of using ultra-narrow band filter (UNBF) has been investigated and compared to that of conventional interference filter, with the aim of reducing background noise in daytime measurements and improving the transmission of the useful signal. The results show that the photon counting acquisition technique for a DIAL system or P-DIAL (Photon-counting DIAL) provides superior performance in terms of signal quality and measurement accuracy compared to analogue detection using an UNBF for noise limitation.

Keywords

DIAL, Lidar, Detection, Noise, Photon Counting, UNBF

1. Introduction

Photon-counting lidar aims to achieve performance comparable to that of traditional waveform-based systems. It employs a high-repetition micro-pulse laser along with highly sensitive single-photon detectors to capture returned signals at the single-photon level. This approach enables the detection of distant spatial targets while requiring lower laser energy. [1, 2] Based on direct absorption (Beer–Lambert law) and a ratio of two signals [3], the P-DIAL (Photon counting DIAL) technique is an active remote sensing method that uses individual photon counting to analyse atmospheric properties

*Corresponding author: hajanirinajeanemile@gmail.com (Hajanirina Jean Emile Randrianjatovo)

Received: 7 October 2025; **Accepted:** 20 October 2025; **Published:** 26 November 2025

such as gas concentration.

To perform measurements using this technique, it is crucial to study its performance as a function of the emission, reception and detection (or acquisition) parameters, which are characteristic modules of a lidar system. [4] The results of this study indicate that P-DIAL is a reliable and sensitive technique for monitoring atmospheric gases and for environmental remote sensing applications.

2. Materials and Methods

LIDAR (Light Detection and Ranging) is a technology similar to RADAR (Radio Detection And Ranging), except that it uses light emitted by a laser [5]. When combined with the differential absorption technique and photon-counting detection, it becomes a powerful tool for addressing a major scientific and environmental challenge.

2.1. Lidar Equation

The main advantage of lidar over other optical instruments is its ability to provide vertical profiles, i.e. to measure the variation of a parameter as a function of distance from the emitting system.

As a function of distance R, the backscattered optical power is given by [6]:

$$P(R,\lambda) = \frac{c\tau}{2} P_0 A \eta_s \frac{O(R)}{R^2} \beta(R,\lambda) \exp\left[-2\int_0^R \alpha(z,\lambda)dz\right] \quad (1)$$

The parameters used in the lidar equation are presented in Table 1.

Table 1. *Lidar system paramters.*

Parameters	Signification
c	Speed of light [m.s^{-1}]
τ	Pulse duration [s]
P_0	Laser pulse power [W]
A	Receiver telescope area [m^2]
η_s	System efficiency
$O(R)$	Receiver fied of view overlap factor
$\beta(R,\lambda)$	Backscatter coefficient [m^{-1}sr^{-1}]
$\alpha(z,\lambda)$	Extinction coefficient [m^{-1}]

2.1.1. Backscatter Coefficient

The backscatter coefficient is the main atmospheric parameter that determines the intensity of the lidar signal. It describes the amount of light returned to the lidar receiver, including contributions from molecular scattering and aerosols. [7].

$$\beta(\lambda,z) = \beta_{mol}(z,\lambda) + \beta_{aer}(z,\lambda) \quad (2)$$

The molecular backscatter coefficient $\beta_{mol}(z,\lambda)$ and the aerosol backscatter coefficient are expressed as follows:

$$\begin{cases} \beta_{mol}(z,\lambda) = \frac{p(z)}{k_B T(z)}\sigma_{mol} = 5.45 \times 10^{-32}\left(\frac{\lambda_0}{\lambda}\right)^4 \frac{p(z)}{k_B T(z)} \\ \beta_{aer}(\lambda) = \int_0^\infty \pi a^2 Q_{back}(k_p,m) N_{aer}(a) da \end{cases} \quad (3)$$

Where σ_{mol} is the molecular scattering cross-section, λ_0 = 550 nm (a reference wavelength), λ is the emission wavelength in nm, $p(z)$ and $T(z)$ denote the pressure and temperature at altitude z, respectively, k_B is the Boltzmann constant, a is the aerosol radius, $Q_{back(k_p,m)}$ is the backscatter efficiency, k_p is the particle size, m is the complex refractive index, and $N_{aer}(a)$ is the aerosol number density.

2.1.2. Extinction Coefficient

The extinction coefficient results from the absorption and scattering of atmospheric constituents (molecules and aerosols). [7].

$$\alpha(z,\lambda) = \alpha_{aer}(z,\lambda) + \alpha_{mol}(z,\lambda) \quad (4)$$

The expressions of $\alpha_{aer}(z,\lambda)$ and $\alpha_{mol}(z,\lambda)$ are given using equation (5).

$$\begin{cases} \alpha_{aer}(z,\lambda) = \alpha_{aer,diff} + \alpha_{aer,abs} \\ \alpha_{mol}(z,\lambda) = \alpha_{mol,diff} + \alpha_{mol,abs} \end{cases} \quad (5)$$

Where $\alpha_{aer,diff}$ and $\alpha_{mol,diff}$ are respectively the extinction coefficients due to scattering by aerosols and molecules, while $\alpha_{aer,abs}$ and $\alpha_{mol,abs}$ are due to absorption mechanisms. We have:

$$\begin{cases} \alpha_{aer} = \int_0^\infty \pi a^2 Q_{ext}(k_p,m) N_{aer}(a) da \\ \alpha_{mol}(z) = \frac{8\pi}{3}\beta_{mol}(z) \end{cases} \quad (6)$$

2.2. DIAL Technique

The DIAL system is based on the alternate emission of two laser pulses [8]:

1) An absorption wavelength (λ_{on}) strongly absorbed by the target gas,
2) A wavelength outside the absorption line of the target gas (λ_{off}).

The equation relating these two wavelengths is:

$$N_{mol}(R) = \frac{1}{2\Delta\sigma_{abs}}\left[\frac{d}{dR}\ln\left(\frac{P(R,\lambda_{off})}{P(R,\lambda_{on})}\right)\right] \quad (7)$$

Where $N_{mol}(R)$ represents the gas molecular density (molecules/m^3) and σ_{abs} is the molecular absorption cross-section.

σ_{abs} quantifies the probability that a photon will be absorbed by a given molecule at a specific frequency υ or wavelength. [9].

$$\sigma_{abs}(\upsilon, T, p) = \sum_k S_k(T).\, g_k(\upsilon - \upsilon_0, T, p) \quad (8)$$

Where $S_k(T)$ denotes the line intensity depending on temperature, and $g_k(\upsilon)$ is the line shape function, such that:

$$\begin{cases} S_k(T, \upsilon_0) = S_k(T_0, \upsilon_0).\left(\frac{T_0}{T}\right)^{\frac{3}{2}}.\exp\left[-\frac{hcE''}{k_B}\left(\frac{1}{T} - \frac{1}{T_0}\right)\right] \\ \int_0^\infty g_k(\upsilon - \upsilon_0, T, p) = 1 \end{cases} \quad (9)$$

Where $S_k(T_0, \upsilon_0)$ is the transition intensity at the reference temperature, conventionally set to $T_0 = 296\,K$ in the HITRAN (High-resolution Transmission molecular absorption) database, E" denotes the ground state energy associated with the considered transition, and h is Planck's constant.

The following Figure 1 illustrates the CO_2 absorption cross-section at 2 µm obtained from spectroscopic measurements carried out by PNNL (Pacific Northwest National Laboratory). [10].

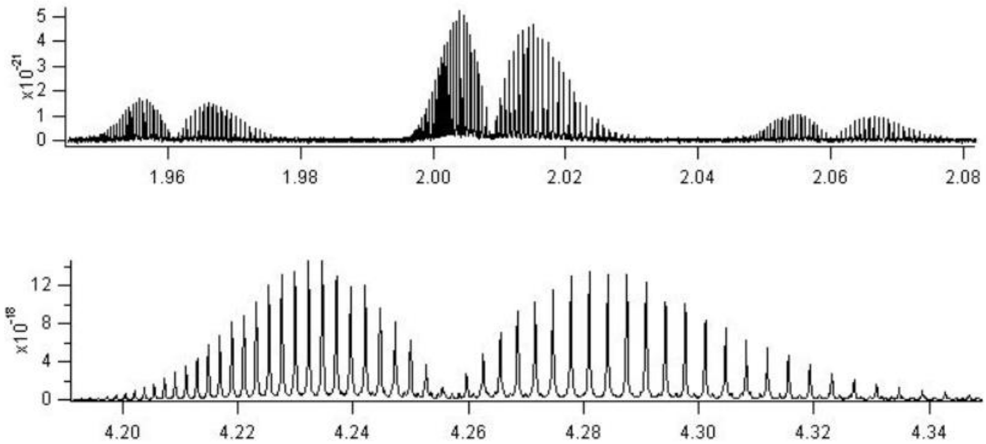

Figure 1. *Molecular absorption cross-section of CO_2 in the 2.05 µm and 4.3 µm band.*

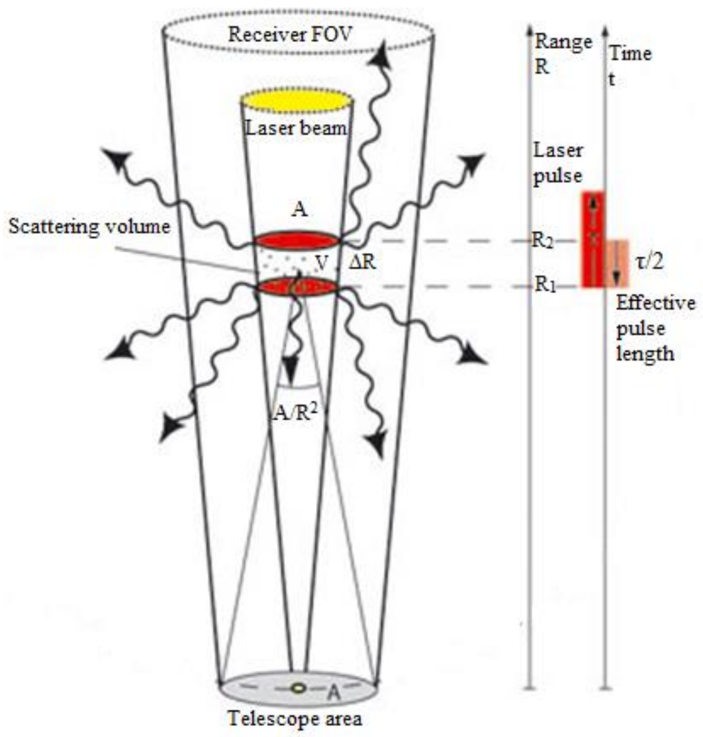

Figure 2. *Geometry of SPL.*

2.3. Single Photon Counting LIDAR (SPL)

Equation (10) defines the number of received photons originating from a volumetric scattering layer for a single laser shot. [11].

$$N_d(\lambda, R) = \left(\frac{\eta P_0}{hf}\right) \beta(\lambda, R) \Delta R \frac{A}{R^2} O(R) T^2(\lambda, R) \eta_{rx} \eta_{tx} \quad (10)$$

Where f denotes the frequency in Hz, ΔR is the range resolution, and η_{rx} and η_{tx} are the reception and transmission efficiencies, respectively. [12].

Figure 2 shows the geometry of the SPL, illustrating some parameters included in the single photon counting lidar equation.

2.4. Photon Counting DIAL (P-DIAL)

The design of a P-DIAL (See Figure 3) system requires several devices, each with its key roles, summarized in Table 2.

Table 2. Devices and their roles in a P-DIAL system.

Devices	Roles
Laser source	Generates light beams at two distinct wavelengths
Beam expander	Increases the laser beam diameter while reducing its divergence
Transmitting telescope	Focuses and directs the laser beam toward the target
Receiving telescope	Captures the backscattered light from atmospheric molecules or particles
Optical filter	Isolates the wavelengths corresponding to the laser beams
Photon detectors (PMT or SPAD)	Convert the backscattered photons into electrical pulses
Electrical recording system	Records the arrival time of photons

Figure 3 illustrates the basic architecture of a photon-counting DIAL system.

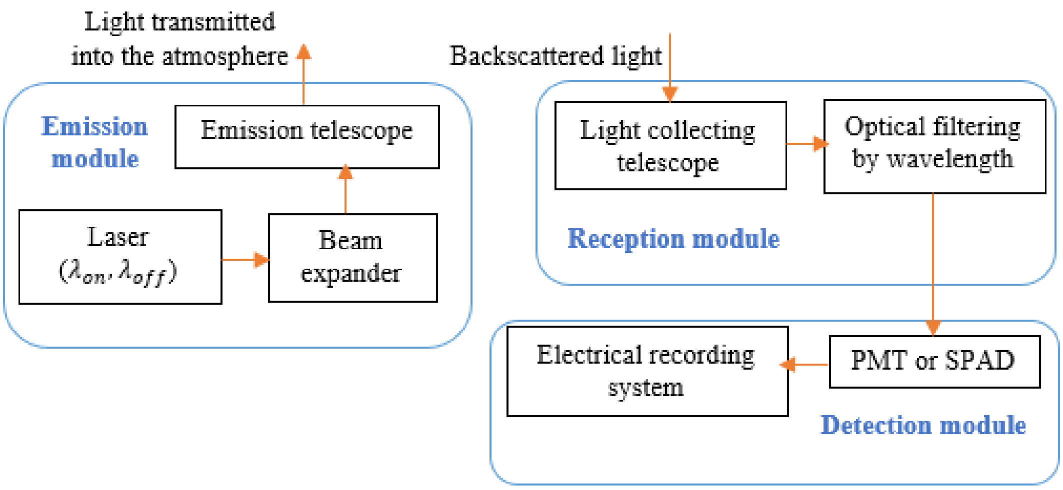

Figure 3. Architecture of P-DIAL.

2.4.1. P-DIAL Equation

By including the absorption term, the corresponding equation for the number of photons received at wavelength λ can be rewritten in the form:

$$N_d(\lambda, R) = \left(\frac{\eta P_0}{hf}\right) \eta_{rx} \eta_{tx} \beta(\lambda, R) \Delta R \frac{A}{R^2} O(R) \exp\left[-2\int_0^{R_1} [\beta_{diff}(\lambda, z) + \gamma(\lambda, z)] dz\right] \exp\left[-2\int_{R_1}^{R} [\beta_{diff}(\lambda, z) + \gamma(\lambda, z)] dz\right] \quad (11)$$

Where $\gamma(\lambda, z)$ is the absorption coefficient and R_1 is the distance representing the starting point of the path along which the unknown gas concentration is measured.

If we set $C_0 = \left(\frac{\eta P_0}{hf}\right)\eta_{rx}\eta_{tx}\Delta R \frac{A}{R^2} O(R)$, we obtain:

$$N_d(\lambda, R) = C_0\beta(\lambda, R) \exp\left[-2\int_0^{R_1}[\beta_{diff}(\lambda, z) + \gamma(\lambda, z)]dz\right] \exp\left[-2\int_{R_1}^{R}[\beta_{diff}(\lambda, z) + \gamma(\lambda, z)]dz\right] \tag{12}$$

The concentration profile of the unknown gas N_{mol} is derived from the ratio of the number of received photons $N_d(\lambda_{on})$ and $N_d(\lambda_{off})$.

$$\frac{N_d(\lambda_{on},R)}{N_d(\lambda_{off},R)} = \frac{C_{0,on}}{C_{0,off}}\left[\frac{\beta(\lambda_{on},R)}{\beta(\lambda_{off},R)}\right] \exp\left\{-2\int_{R_1}^{R}[\Delta\sigma_{abs}N_{mol}(z) + \beta_{diff}(\lambda_{on}, z) - \beta_{diff}(\lambda_{off}, z)]dz\right\} \tag{13}$$

If we assume that $C_{0,off} = C_{0,on}$, equation (13) becomes:

$$\frac{N_d(\lambda_{on},R)}{N_d(\lambda_{off},R)} = \left[\frac{\beta(\lambda_{on},R)}{\beta(\lambda_{off},R)}\right] \exp\left\{-2\int_{R_1}^{R}[\Delta\sigma_{abs}N_{mol}(z) + \beta_{diff}(\lambda_{on}, z) - \beta_{diff}(\lambda_{off}, z)]dz\right\} \tag{14}$$

Consequently, in P-DIAL measurements, the concentration of the absorbing gas $N_{mol}(R)$ can be determined from equation (14) and is expressed using equation (15).

$$N_{mol}(\mathrm{R}) = \frac{1}{2\Delta\sigma_{abs}}\left\{\frac{d}{dR}\left[\ln\frac{N_d(\lambda_{off},R)}{N_d(\lambda_{on},R)}\right]\right\} + \frac{1}{2\Delta\sigma_{abs}}\left\{\frac{d}{dR}\left[\ln\frac{\beta(\lambda_{on},R)}{\beta(\lambda_{off},R)}\right]\right\} - \frac{1}{\Delta\sigma_{abs}}[\beta_{diff}(\lambda_{on}, R) - \beta_{diff}(\lambda_{off}, R)] \tag{15}$$

The first term, denoted as $N'_{mol}(R)$, represents the fundamental term that is directly determined from the signal ratio as follows:

$$N'_{mol}(R) = \frac{1}{2\Delta\sigma_{abs}}\frac{d}{dR}\ln\left[\frac{N_d(\lambda_{off},R)}{N_d(\lambda_{on},R)}\right] \tag{16}$$

By expressing the derivative in terms of a distance increment R, the average value $N'_{mol}(R + \Delta R)$, simplified as $N'_{mol}(R)$, is obtained as follows:

$$N'_{mol}(R) = \frac{1}{2\Delta\mathrm{R}\Delta\sigma_{abs}}\left[\ln\frac{N_d(\lambda_{on},R)}{N_d(\lambda_{on},R+\Delta R)} - \ln\frac{N_d(\lambda_{off},R)}{N_d(\lambda_{off},R+\Delta R)}\right] \tag{17}$$

The gas concentration (kg.m^{-3} or g.m^{-3}), denoted as C, is calculated by multiplying equation (17) by the molecular mass M.

$$C = M.N'_{mol}(R) = \frac{M}{2\Delta\mathrm{R}\Delta\sigma_{abs}}\left[\ln\frac{N_d(\lambda_{on},R)}{N_d(\lambda_{on},R+\Delta R)} - \ln\frac{N_d(\lambda_{off},R)}{N_d(\lambda_{off},R+\Delta R)}\right] \tag{18}$$

2.4.2. Relative Error of the Concentration

By considering that the error in the off-signal is negligible [13], $N'_{mol}(R)$ can then be expressed as follows:

$$N'_{mol}(R) = \frac{1}{2\Delta\mathrm{R}\Delta\sigma_{abs}}[\ln N_d(\lambda_{on}, R) - \ln N_d(\lambda_{on}, R + \Delta R)] \tag{19}$$

The relative error of the chemical species concentration is denoted as $\delta N'$ and is defined as:

$$\delta N' = \frac{\delta N'_{mol}}{N_{mol}} \tag{20}$$

To calculate the uncertainty $\delta N'$, the error propagation formula is applied, which takes into account the variations of the signals $N_d(\lambda_{on}, R)$ and $N_d(\lambda_{on}, R + \Delta R)$. For simplicity, we denote $N_d(\lambda_{on}, R) = N_{on}(R)$ and $N_d(\lambda_{on}, R + \Delta R) = N_{on}(R + \Delta R)$.

The uncertainty $\delta N'_{mol}$ can then be determined as follows:

$$\delta N'_{mol} = \sqrt{\left[\frac{\partial N'_{mol}(R)}{\partial N_{on}(R)}\delta N_{on}(R)\right]^2 + \left[\frac{\partial N'_{mol}(R)}{\partial N_{on}(R+\Delta R)}\delta N_{on}(R+\Delta R)\right]^2} \quad (21)$$

By differentiating $N'_{mol}(R)$ compared to $N_{on}(R)$ and $N_{on}(R+\Delta R)$, we obtain:

$$\frac{\partial N'_{mol}(R)}{\partial N_{on}(R)} = \frac{1}{2\Delta R\Delta\sigma_{abs}}\frac{1}{N_{on}(R)}$$

$$\frac{\partial N'_{mol}(R)}{\partial N_{on}(R+\Delta R)} = -\frac{1}{2\Delta R\Delta\sigma_{abs}}\frac{1}{N_{on}(R+\Delta R)}$$

Equation (21) then leads to the following expression:

$$\delta N'_{mol} = \sqrt{\left[\frac{1}{2\Delta R\Delta\sigma_{abs}}\frac{1}{N_{on}(R)}\delta N_{on}(R)\right]^2 + \left[-\frac{1}{2\Delta R\Delta\sigma_{abs}}\frac{1}{N_{on}(R+\Delta R)}\delta N_{on}(R+\Delta R)\right]^2} \quad (22)$$

By factoring out $\frac{1}{2\Delta R\Delta\sigma_{abs}}$, we obtain the equation:

$$\delta N'_{mol} = \frac{1}{2\Delta R\Delta\sigma_{abs}}\sqrt{\left[\frac{\delta N_{on}(R)}{N_{on}(R)}\right]^2 + \left[\frac{\delta N_{on}(R+\Delta R)}{N_{on}(R+\Delta R)}\right]^2} \quad (23)$$

For small ΔR, the quantities $N_d(\lambda_{on}, R)$ and $N_d(\lambda_{on}, R+\Delta R)$ may be highly correlated. Therefore, the covariance term $Cov[N_d(R), N_d(R+\Delta R)]$ is included into equation (23), yielding:

$$\delta N'_{mol} = \frac{1}{2\Delta R\Delta\sigma_{abs}}\sqrt{\left[\frac{\delta N_{on}(R)}{N_{on}(R)}\right]^2 + \left[\frac{\delta N_{on}(R+\Delta R)}{N_{on}(R+\Delta R)}\right]^2 \pm Cov\big(N_{on}(R), N_{on}(R+\Delta R)\big)} \quad (24)$$

Finally, from equation (20), we obtain:

$$\delta N' = \frac{1}{2N_{mol}(R)\Delta R\Delta\sigma_{abs}}\sqrt{\left[\frac{\delta N_{on}(R)}{N_{on}(R)}\right]^2 + \left[\frac{\delta N_{on}(R+\Delta R)}{N_{on}(R+\Delta R)}\right]^2 \pm Cov\big(N_{on}(R), N_{on}(R+\Delta R)\big)} \quad (25)$$

2.5. SNR

In photon-counting techniques, including P-DIAL, only zero (no photon detected) or positive integer values are recorded. Due to this characteristic, the estimation of statistical error is based on the assumption that the uncertainty in the number of photons detected by the photodetector follows a Poisson distribution [14]. Under this assumption, the SNR is expressed using the following equation [15]:

$$SNR_\lambda(R) = \frac{N_d(\lambda,R)}{\sqrt{N_d(\lambda,R)+N_B+N_C}} \quad (26)$$

Where N_B and N_C represent, respectively, the number of counts due to background noise and the fluctuations of the photodetector's dark current during the interval $2\Delta R/c$.

The number of photons from the background light received by the lidar can be expressed as follows:

$$N_B = \left(\pi\frac{A.D}{hf}\right)\left(\frac{{\theta_t}^2}{4}\right)\eta_{rx}\eta_f\eta L_c(\lambda)\Delta t \quad (27)$$

Where η_f is the efficiency of the background-noise-limiting filter, $L_c(\lambda)$ is the radiance of the sky background noise, D is the bandwidth of the filter, θ_t is the field of view (FOV) of the telescope, Δt denotes the time during which the background light can be received and η is the quantum efficiency of the photodetector used.

2.6. Optical Filtering Techniques

The P-DIAL should be capable of performing measurements efficiently, whether at night or during the day. Indeed, due to the intensity of solar radiation during daytime, the daytime SNR is much lower than the nighttime SNR; altitude and detection accuracy are also strongly limited [16]. Almost all lidars use interference filters to address the main issue of limiting sky background noise in daytime measurements. However, studies indicate that an ultra-narrow band filter (UNBF) provides a higher SNR than an interference filter. The structure of a UNBF is illustrated in Figure 4.

To maximize the suppression of solar background noise during daytime measurements, two Fabry–Perot interferometers (FPIs) with different resolutions (Low Resolution and High Resolution) are cascaded with the interference filter (IF). This configuration narrows the transmission to a single band across the IF's spectral range, providing enhanced noise filtering efficiency.

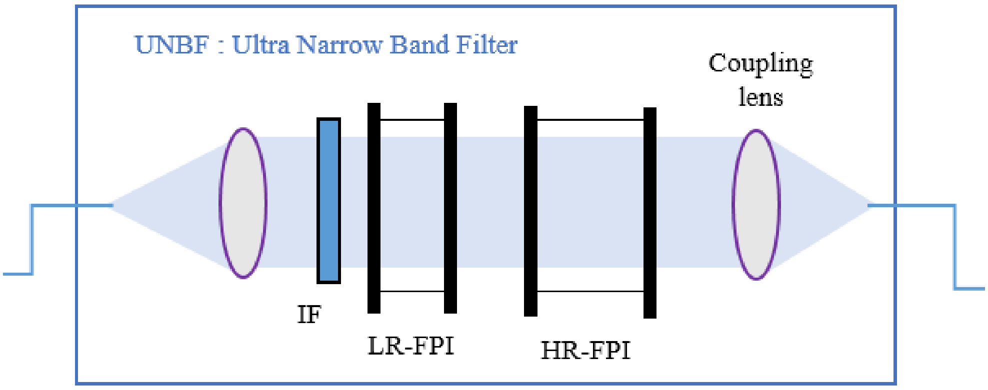

Figure 4. *UNBF optical structure.*

The transmission of the interference filter and the FPI are described respectively by equations (28) and (29). [17].

$$T_{IF}(\lambda) = \frac{1}{1+M_f \sin^2\left(\frac{2\pi n_e d.\cos\theta}{\lambda}\right)} \quad (28)$$

Where M_f is the modulation factor, n_e is the effective refractive index of the filter material, d is the thickness of the optical layers, and θ is the angle of incidence of the light on the filter.

$$T_{FPI}(\lambda) = T_{max}\frac{1-R_{FP}}{1+R_{FP}}\left[1+2\sum_{n=1}^{\infty} R_{FP}{}^{n}\left[\frac{2\pi n_{FP}}{\lambda.FSR}\frac{1+\cos\theta}{2}\right]\sin c\left[\frac{2n_{FP}}{\lambda_0.FSR}\frac{1-\cos\theta}{2}\right]\right] \quad (29)$$

Where T_{max} is the maximum transmission, R_{FP} is the effective reflectivity of the FPI plates, n_{FP} is the refractive index of the medium between the two FPI plates, FSR is the free spectral range of the FPI, θ is the beam divergence angle and λ_0 is the laser wavelength.

The total transmission of the filter assembly for reducing solar background radiation across the wavelength range is:

$$T_{UNBF}(\lambda) = T_{IF}(\lambda).T_{LRFPI}(\lambda).T_{HRFPI}(\lambda) \quad (30)$$

2.7. Performance Criteria

The performance of the P-DIAL system depends on the properties of the components used at the source, receiver and detector (Table 3). However, it is also necessary to consider atmospheric influences.

Table 3. *Important parameters in measurement.*

Module	Parameters
Emission	Laser pulse duration τ Resolution ΔR Spectral width $\Delta\nu$ Pulse repetition frequency Energy
Reception	Collecting optics area Field of view (FOV) Spectral width of the optical filter
Detection	SPDE (Single Photon Detection Efficiency) Dark count rate

3. Results

The results are obtained from MATLAB simulations of the different parameters by analyzing their impacts on the SNR in equation (26).

Some values used in the simulation are presented in the following table.

Table 4. *Values of parameters used in the simulation.*

Parameters	Values
Backscatter coefficient	10^{-7} $m^{-1}sr^{-1}$ [18]
On-line wavelength	2050 nm
Off-line wavelength	2056 nm
Pulse duration	30 ns
Laser energy	10 mJ
Diameter of the telescope	30 cm
Receiver fied of view overlap factor	0.6
Dark count	100 kcps
FOV	8 mrad
Filter bandwidth	500 nm
SPDE	0.7

3.1. SNR of the P-DIAL and the Analog DIAL

The SNR is a crucial parameter used to assess the signal quality of a system in relation to the noise level.

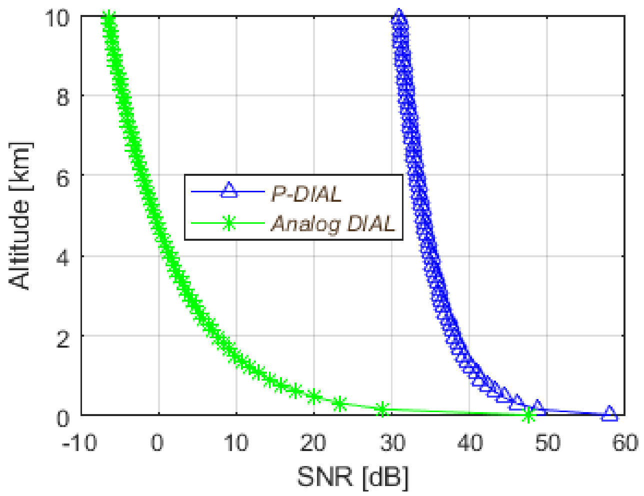

Figure 5. *SNR profile for P-DIAL and analogic DIAL.*

The presented curves highlight that the SNR of the P-DIAL system significantly outperforms that of the conventional DIAL, thereby demonstrating the efficiency and superiority of the photon-counting approach. Furthermore, a gradual decrease in SNR is observed with increasing altitude, reflecting the signal attenuation caused by various noise sources affecting the measurements.

3.2. Performance of the Filters

The following Figure 6 illustrates the SNR profile used to compare the performance of the interference filter and the UNBF.

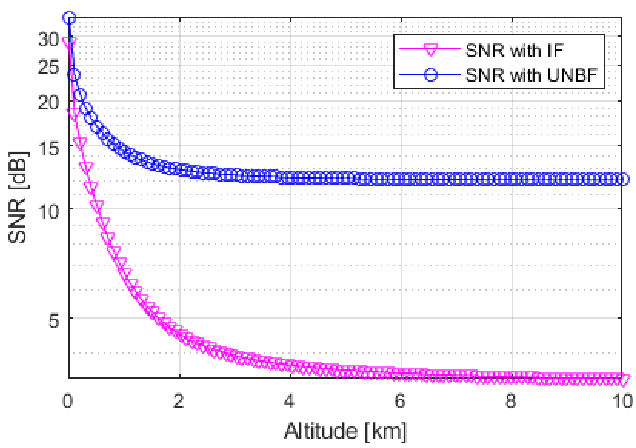

Figure 6. *SNR profile using the IF and the UNBF.*

Taking into account background noise, i.e., under daytime measurements, the simulation result illustrated in Figure 6 highlights that the use of an ultra-narrow band filter (UNBF) significantly improves the signal-to-noise ratio compared to using only the interference filter, since the SNR with the UNBF is higher than that of the IF. Thus, the IF is outperformed by the UNBF due to the combination of multiple filters, which provides optimized transmission of the useful wavelength and strong rejection of background noise. Therefore, the use of the UNBF offers superior performance under daytime conditions.

3.3. Influence of Source-level Parameters

The studies are based on the laser pulse duration (Figure 7a), spectral width (Figure 7b), repetition frequency (Figure 7c), and energy (Figure 7d). Figure 7 shows the SNR as a function of these parameters.

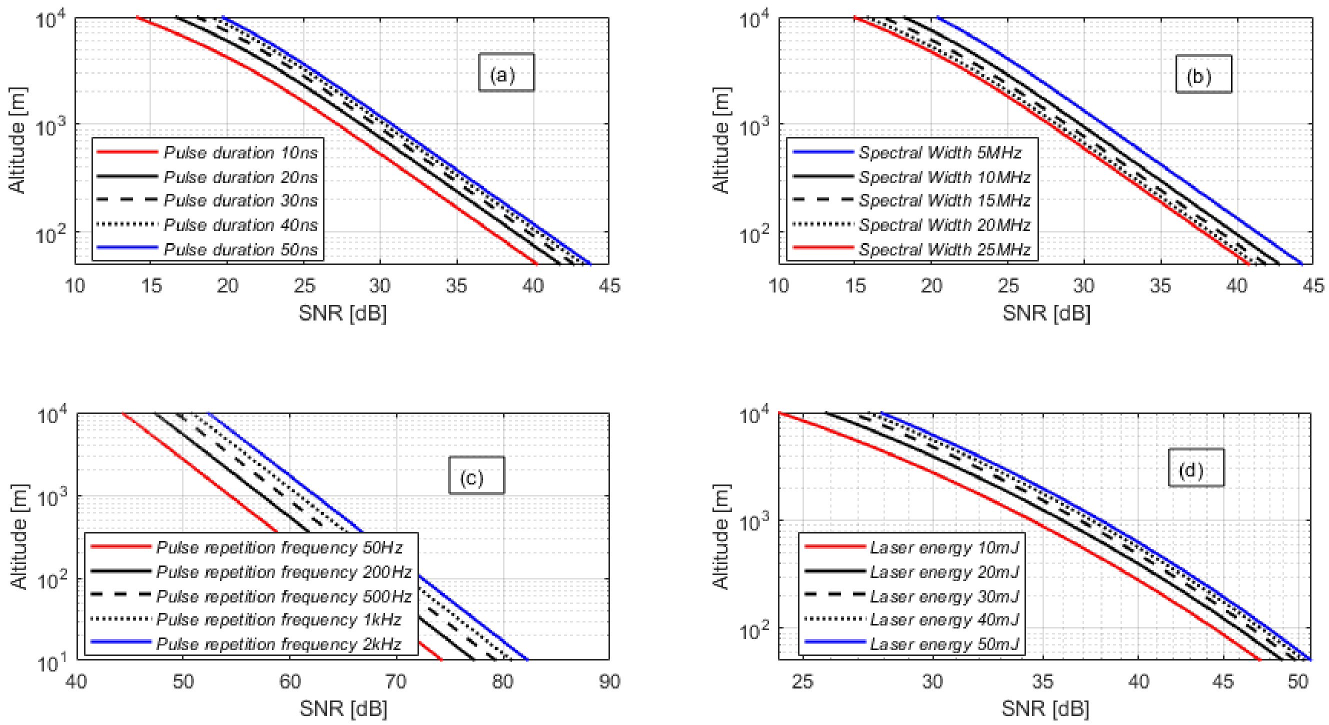

Figure 7. *SNR profile for different emission parameter values.*

All these parameters influence the SNR. It depends strongly on the pulse duration: a shorter pulse improves spatial resolution but reduces the energy per pulse, which degrades the SNR. In our study, a 50 ns pulse provides a better compromise than a 10 ns pulse. Furthermore, laser energy is a key parameter that determines the measurement range and quality, as higher energy increases the number of detected photons and improves the SNR, while too low an energy significantly reduces the useful range and accuracy. The laser spectral width also has a significant impact on the SNR, especially when it is narrower. Finally, a reliable SNR is also achieved at a high repetition frequency.

3.4. Influence of Parameters at the Receiver Level

The receiving chain (telescope, optical filter) also plays a decisive role in the SNR and therefore in the performance of the measurement. The results are presented in Figure 8 (Figure 8a for the FOV, Figure 8b for the spectral width of the optical filter, Figure 8c for the aperture diameter of the telescope).

The results indicate that the field of view (FOV) and the telescope diameter have a significant impact on the SNR. A wide FOV, such as 8 mrad in Figure 8a, allows the collection of a larger photon flux, leading to a slight improvement in the SNR compared to a narrow FOV, like the 1.5 mrad used in our simulation. Moreover, the influence of the telescope diameter on the SNR profile is also evident. A larger aperture enables the collection of more photons reflected from the target, which directly increases the detected photon flux. This enhancement of the measured signal results in a significant rise in SNR. Finally, the simulation results shown in Figure 8c demonstrate that a bandwidth below 50 nm is an optimal choice, as it effectively suppresses spectral background noise while preserving the transmission of the DIAL line.

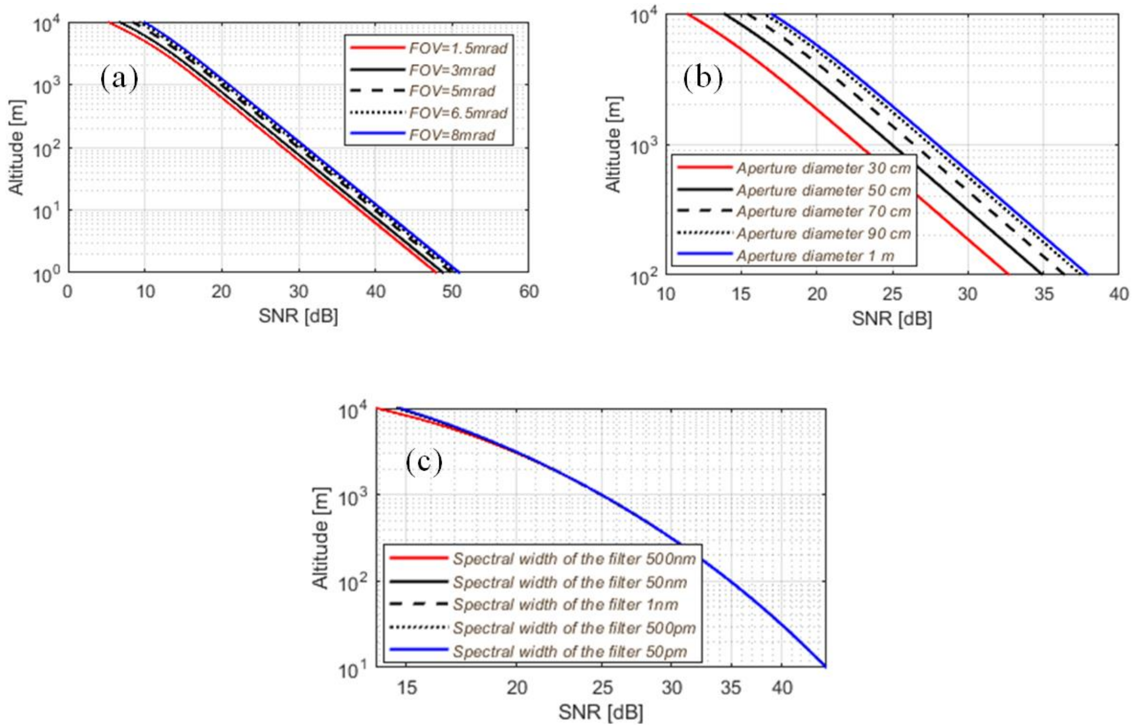

Figure 8. *SNR profile for telescope and optical filter parameters.*

3.5. Influence of Parameters at the Detector Level

Figure 9 shows the influence of SPDE on the SNR of P-DIAL. The single photon detection efficiency (SPDE) influences the SNR, but its impact remains limited in the range studied. The differences observed between low and high efficiency values remain relatively small. Nevertheless, when the SPDE is high, the conversion of incident photons into detected events improves, thereby strengthening the robustness of the signal.

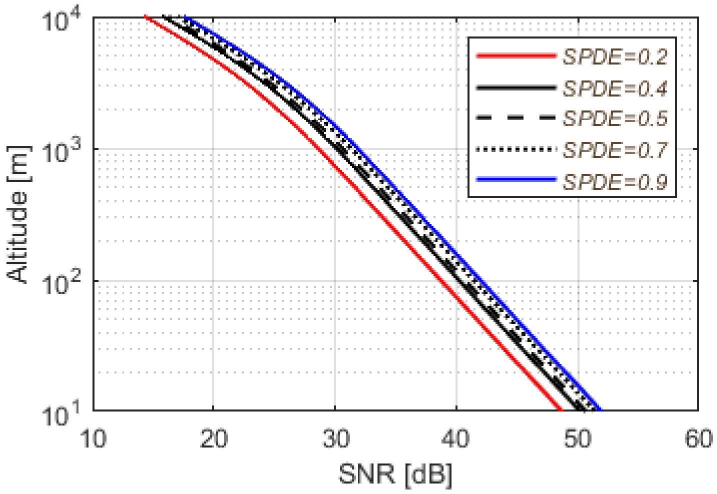

Figure 9. *SNR profile for several values of SPDE.*

3.6. Influence of Atmospheric Parameters

The atmospheric parameters that influence the SNR are $\beta_{mol}(z)$ and $\alpha_{mol}(z)$ in the lidar equation, and since they depend on temperature and pressure, we will also present the results of the SNR profile as a function of these two parameters.

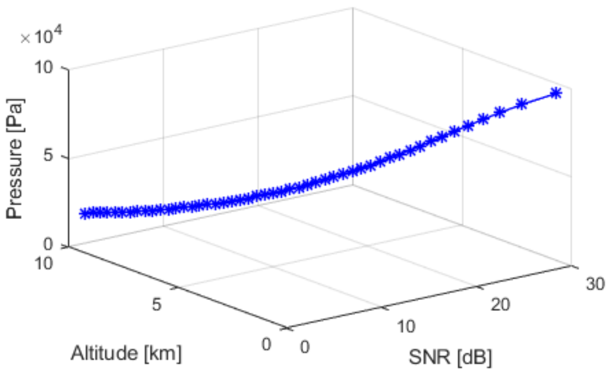

Figure 10. *SNR profile as a function of altitude and pressure.*

Atmospheric pressure decreases with altitude, and the SNR of the P-DIAL system also tends to decrease as altitude increases (Figure 10). Conversely, higher pressure promotes better detection efficiency, which translates into improved SNR. Moreover, Figure 11 illustrates the SNR curve as a function of temperature.

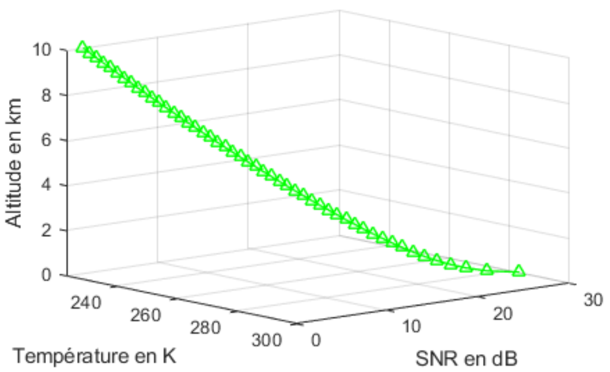

Figure 11. *SNR profile as a function of temperature.*

The result highlights the impact of temperature on the SNR. The SNR values increases as the temperature rises.

For cases $\beta_{mol}(z)$ and $\alpha_{mol}(z)$, Figure 12 shows the SNR curve as a function of these two parameters.

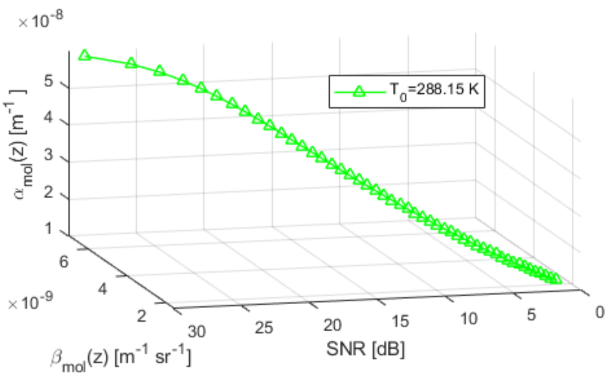

Figure 12. *SNR profile based on backscatter and extinction coefficients.*

It appears that the SNR increases when the values of the two coefficients considered increase. This highlights the decisive role of molecular backscattering and extinction coefficients in the overall performance of the P-DIAL system.

3.7. Choice of Wavelengths

The choice of wavelengths is linked to the availability of laser sources and the absorption lines of gases. Figure 13 shows an example of the choice of two wavelengths for CO_2 at 2.05 µm using equations (8) and (9).

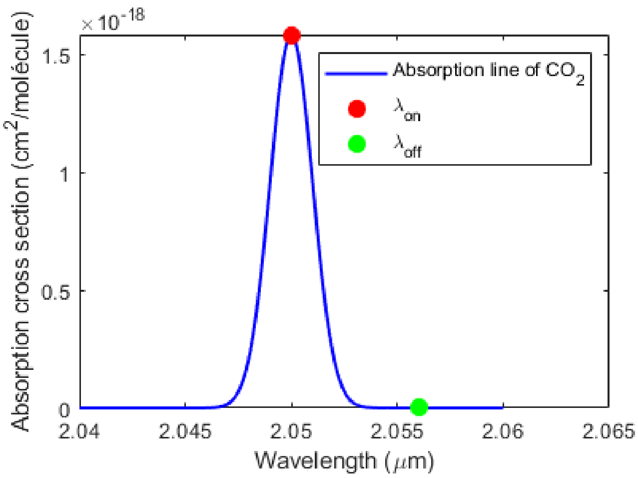

Figure 13. *Absorption line of CO_2 and positions of λ_{on} and λ_{off}.*

3.8. Number of Photons Detected at λ_{on} and λ_{off}

Let us again consider the case of CO_2. The wavelength of 2.05 µm corresponds to strong absorption for CO_2. The objective is to illustrate that the number of photons detected (See Equation (10)) at λ_{on} is attenuated compared to those detected at λ_{off} due to the absorption effect.

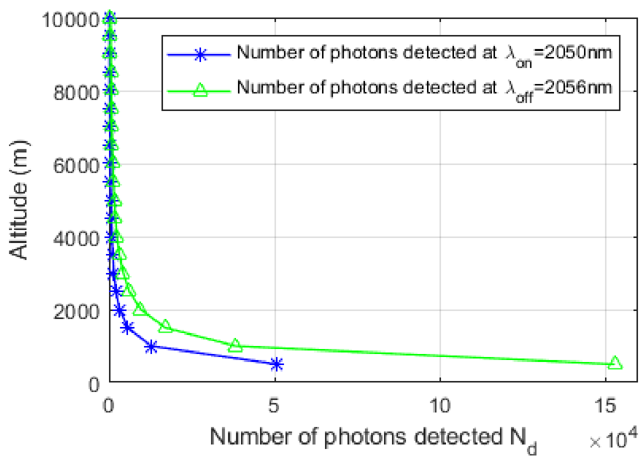

Figure 14. *Profile of the number of photons detected.*

Due to the absorption effect, atmospheric transmission at λ_{on} is lower than that at λ_{off}.

4. Discussion

In this study, the reference altitude was set at 10 km, corresponding to the tropospheric region where satisfactory SNR values were obtained. However, the implementation of the P-DIAL measurement requires consideration of a set of parameters, ranging from the emission of the laser radiation to photon-counting detection, while also accounting for atmospheric conditions.

Our theoretical analysis provided a better understanding of how the system works and enabled us to evaluate its performance, particularly by studying the SNR as a function of instrumental and atmospheric parameters. The results obtained confirm the reliability of photon-counting acquisition within the framework of the DIAL technique.

Nevertheless, for experimental implementation, the choice of components must be tailored to the system's requirements, particularly regarding the type of detector (to avoid saturation when the incoming photon flux is high) and the laser source, a central element since the development of lidar has relied precisely on its exploitation.

Finally, this study was limited to the use of two wavelengths. However, in order to probe different absorption lines or target multiple gases, it is necessary to resort to multispectral measurement, which imposes stricter requirements in terms of spectral stability and optical filtering.

5. Conclusion

Due to the growing importance of atmospheric sounding in the current context, the work presented in this manuscript carries significant value as it addresses both societal and environmental issues, namely the monitoring of tropospheric gases. A thorough analysis of the parameters influencing the performance of a P-DIAL system is essential, as it guides the selection of instrumental components based on the optimal characteristics identified through simulations.

Furthermore, the experimental implementation of such a system requires precise knowledge of the spectroscopic properties of the target gases, in order to properly adapt the operating wavelengths and account for real atmospheric conditions that affect absorption and scattering.

Abbreviations

DIAL	Differential Absorption Lidar
LIDAR	Light Detection and Ranging
P-DIAL	Photon Counting DIAL
RADAR	Radio Detection And Ranging
GHGs	Greenhouse Gases
HITRAN	High Resolution Transmission
PNNL	Pacific Northwest National Laboratory
SPL	Single Photon Lidar
SNR	Signal to Noise Ratio
UNBF	Ultra Narrow Band Filter
FPI	Fabry-Perot Interferometer
IF	Interference Filter
LR-FPI	Low Resolution FPI
HR-FPI	High Resolution FPI
FOV	Field of View
SPDE	Single Photon Detection Efficiency

Author Contributions

Hajanirina Jean Emile Randrianjatovo: Conceptualization, Data curation, Formal analysis, Investigation, Writing – review & editing.

Hariniony Bienvenu Rakotonirina: Funding acquisition, Supervision.

Marie Emile Randrianandrasana: Methodology, Project administration, Validation, Visualisation.

Funding

This work is not supported by any external funding.

Data Availability Statement

The data is available from the corresponding author upon reasonable request.

Conflicts of Interest

The authors declare no conflicts of interest.

References

[1] Z. Wang, M. Menenti. Challenges and opportunities in Lidar remote sensing. Frontiers in Remote Sensing. 2022. https://doi.org/10.3389/frsen.2021.641723

[2] C. Wang, X. Yang, X. Xi, S. Nie. P. Dong. Introduction to LiDAR remote sensing. CRC Press Boca Raton. 2024, FL, USA. https://doi.org/10.1201/9781032671512

[3] S. M. Spuler, M. Hayman, R. A. Stillwell, J. Carnes, T. Bernatsky, K. S. Repasky. MicroPulse DIAL (MPD)–a diode-laser-based lidar architecture for quantitative atmospheric profiling. Atmospheric Measurement Techniques. 2021. https://doi.org/10.5194/amt-14-4593-2021

[4] C. Klein, «Conception et prototypage d'un lidar pour la mesure du contenu en eau liquide dans le brouillard», phD Thesis, Doctoral School of Sciences of the Universe, Environment and Space (Toulouse). University of Toulouse. 2013.

[5] N. Cezard, «Systèmes LIDAR pour la caractérisation à distance des propriétés physico-chimiques de l'atmosphère», HDR Thesis, Université Fédérale Toulouse Midi-Pyrénées, 2021.

[6] C. Weitkamp. Lidar: range-resolved optical remote sensing of the atmosphere, vol. 102. Springer Science & Business Media. 2005. https://doi.org/10.1007/b106786

[7] J. Shen, N. Cao. Accurate inversion of tropospheric aerosol extinction coefficient profile by Mie-Raman lidar, Optik. 2019, vol. 184, p. 153-164. https://doi.org/10.1016/j.ijleo.2018.12.151

[8] P. Gaudio, M. Gelfusa, A. Malizia, S. Parracino, M. Richetta, L. Leo, C. Perrimezzi, C. Bellecci. Detection and monitoring of pollutant sources with Lidar/Dial techniques, Journal of Physics: Conference Series. 2015, vol. 658, p. 012004. https://doi.org/10.1088/1742-6596/658/1/012004

[9] A. Theopold, J. Bösenberg. Differential Absorption Lidar Measurements of Atmospheric Temperature Profiles: Theory and experiment. Journal of Atmospheric and Oceanic Technology. 1993. https://doi.org/10.1175/1520-0426(1993)010<0165:DALMOA>2.0.CO;2

[10] PNNL (Pacific Northwest Laboratory). CO_2 Absorption Spectra. 2020. https://vpl.astro.washington.edu/spectra/co2pnnlimagesmicrons.htm

[11] H. Xia, G. Shentu, M. Shangguam, X. Xia, X. Jia, C. Wang, J. Zhang, S. Pelc, M. Jefer, Q. Zhang, X. Dou, W. Pan. Long-range micro-pulse aerosol lidar at 1.5 µm with an up-conversion single-photon detector, Optics Letters. 2015, vol. 40, n° 7, p. 1579-1582. https://doi.org/10.1364/OL.40.001579

[12] U. Wandinger. Introduction to Lidar, in *Lidar*, vol. 102, C. Weitkamp, Éd., in Springer Series in Optical Sciences. 2005, vol. 102, New York: Springer-Verlag, p. 1-18. https://doi.org/10.1007/0-387-25101-4_1

[13] V. A. Kovalev, W. E. Eichinger. Elastic lidar: theory, practice, and analysis methods. John Wiley & Sons. 2004. https://doi.org/10.1002/0471643173

[14] P. Gatt, S. Johnson, T. Nichols. Geiger-mode avalanche photodiode ladar receiver performance characteristics and detection statistics. Applied Optics. 2009, vol. 48, n° 17, p. 3261-3276. https://doi.org/10.1364/AO.48.003261

[15] X. Ai, A. Pérez-Serrano, M. Quatrevalet, W. Nock, N. Dahnoun, G. Ehret, I. Esquivias, G. Rarity. Analysis of a random modulation single photon counting differential absorption lidar system for space-borne atmospheric CO_2 sensing, Optics Express. 2016, vol. 24, n° 18, p. 21119-21133. https://doi.org/10.1364/OE.24.021119

[16] F. Han, H. Liu, D. Sun, Y. Han, A. Zhou, N. Zhang, J. Chu, J. Zheng, S. Jiang, Y. Wang. An ultra-narrow bandwidth filter for daytime wind measurement of direct detection Rayleigh lidar. Current Optics and Photonics. 2020, vol. 4, n° 1, p. 69-80. https://doi.org/10.3807/COPP.2020.4.1.069

[17] Y. Han, D. Sun, F. Han, H. Liu, R. Zhao, J. Zhen, N. Zhang, C. Chen, Z. Li. Demonstration of daytime wind measurement by using mobile Rayleigh Doppler Lidar incorporating cascaded Fabry-Perot etalons, Optics Express. 2019, vol. 27, n° 23, p. 34230-34246. https://doi.org/10.1364/OE.27.034230

[18] D. Jones, J. Rothermel. Ground-based measurements of atmospheric backscatter and absorption using coherent CO_2 lidar. Applied Optics. 1985, 3487-3496. https://doi.org/10.1364/AO.24.003487

Research Field

Hajanirina Jean Emile Randrianjatovo: Telecommunication, Remote sensing, Lidar, Optical waves, Signal processing.

Hariniony Bienvenu Rakotonirina: Telecommunication, Signal processing, Compressive sensing, Artificial intelligence, High Amplifier Power Nonlinearity.

Marie Emile Randrianandrasana: Telecommunication, Signal processing, Compressive sensing, Radar, Electromagnetic wave.